

Deformation patterns in thin films under uniform laser irradiation

D. Walgraef

*Mechanical and Aerospace Engineering Department, The University of California at Los Angeles, Los Angeles, California 90024
and Center for Nonlinear Phenomena and Complex Systems, Free University of Brussels, Code Postal 231,
Boulevard du Triomphe, B-1050 Brussels, Belgium*

N. M. Ghoniem

Mechanical and Aerospace Engineering Department, The University of California at Los Angeles, Los Angeles, California 90024

J. Lauzeral

*Center for Nonlinear Phenomena and Complex Systems, Free University of Brussels, Code Postal 231,
Boulevard du Triomphe, B-1050 Brussels, Belgium*

(Received 11 July 1997)

The mechanical behavior of thin films subjected to laser irradiation is described by a dynamical model that is based on coupled evolution equations for the deformation and vacancy density fields. Lattice vacancies are generated in a thin layer as a result of shallow absorption of electromagnetic laser radiation. The strain field associated with lattice dilatation due to vacancies is shown to couple with bending and stretching mechanical deformation fields. The dynamical model developed here is an extension of the work of Emel'yanov in two respects: (1) the coupling between the diffusion and mechanical deformation fields is rigorously developed with additional cross-field contributions; (2) new equations for reduced dynamics are derived from this model, and are used to analyze the physical conditions for the onset of a deformational instability. For a given material, the threshold for this instability is correlated mainly with laser power. We also show that, although the instability threshold and critical wavelengths are given by the linear part of the dynamics, the selection and type of deformation patterns induced by this instability require a nonlinear formulation. Both numerical and analytical analysis are performed here. According to the relative importance of nonlinearities arising from the defect or from the bending dynamics, square or hexagonal planforms are shown to be selected. Furthermore, it appears that one-dimensional gratings are always unstable in isotropic systems. The results for square patterns are consistent with experimental observations, while those for hexagonal and one-dimensional gratings show the importance of anisotropies on their final selection. [S0163-1829(97)03847-2]

I. INTRODUCTION

Laser-induced instabilities are becoming particularly important in several aspects of surface modification technologies. On the one hand, laser-surface interaction may control the structure and properties of thin films, coatings, and semiconductor surfaces. Strong laser radiation induces structural and morphological changes in matter which are responsible for the degradation of light-emitting devices, cumulative laser damage of optical components, and nonuniform melting of semiconductor surfaces, to cite only a few of these aspects.¹⁻⁴ Furthermore, laser annealing and fast recrystallization may lead to special types of structures including molten and crystalline phases, and laser-assisted thin-film deposition processes, which should also be in the mainstream of this activity.⁵ Many of these phenomena proceed through the formation of regular structures on the surface of the material, and laser-surface interaction is evidently a field where patterning phenomena are overwhelming. Hence, the methods of nonlinear dynamics will hopefully lead to a better understanding of the mechanisms of pattern formation, selection, and stability in films and coatings under laser irradiation.

The main instability mechanism in laser-irradiated materials is due to the coupling between defect dynamics and the deformation of the surface.⁶ The interaction of electromag-

netic laser radiation with thin films leads to very strong absorption of photon energy in a shallow layer that is a few wavelengths deep from the surface. As a result, substantial nonequilibrium concentrations of lattice defects are generated. The type of lattice defects depends on the photon energy, wavelength of laser irradiation, and material. Examples of such defects are electron-hole pairs in strongly absorbing semiconductors, interstitials and vacancies in thin films, and voids and dislocation loops in prolonged irradiation. It is the coupling between defect generation, diffusion, and the deformation field that leads to pattern forming instabilities. As a result, the description of such phenomena should be based on the dynamics of the defect field N_d in the thin film and the elastic continuum of the host material described by the displacement vector $\mathbf{U}(\mathbf{r}, t) = (U_x, U_y, U_z)$ with appropriate boundary conditions; both dynamics being coupled through the defect-strain interaction. Various types of defect structures may be induced in such dynamical systems. For example, in the case of thin films under laser irradiation, regular deformation patterns may appear on the film surface when the laser intensity exceeds some threshold. In spatially extended irradiation zones, one- and two-dimensional gratings have been widely observed.^{7,8} In particular, when irradiation proceeds with focused beams, such as in laser-

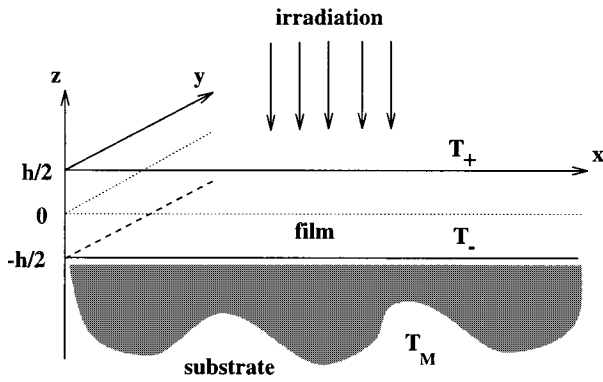


FIG. 1. Geometrical setup of a thin film under laser irradiation.

induced film deposition⁶ or in etching experiments,⁹ roselike deformation patterns are observed, where a finite number of petals develop around a central uniform spot. One striking experimental observation is that the number of petals increases with the intensity of the laser beam.

Our aim in this paper is to perform a dynamical analysis of the formation, selection, and stability of two-dimensional deformation patterns in thin films under uniform laser irradiation. We first develop a dynamical model which leads to deformational instabilities in such systems. This model is an extension of a model first introduced by Emel'yanov.⁶ We also discuss the conditions for instability, while pattern formation beyond the instability threshold is performed through nonlinear analytical and numerical analyses. In Sec. II, we discuss the geometry of the system, and in Sec. III we present a method for calculating temperature distributions in the film. The dynamics of vacancy density evolution are then derived in Sec. IV. On the basis of the first law of thermodynamics, the equation governing the deformation field are given in Sec. V. The stability of undeformed states in weakly adherent films under uniform irradiation is discussed in Sec. VI, while Sec. VII is devoted to weakly nonlinear analysis, amplitude equations, and pattern selection. Finally, numerical results are analyzed in Sec. VIII and conclusions are presented in Sec. IX.

II. LASER IRRADIATION AND THIN-FILM DEFORMATION

The system we consider here represents a thin film on a substrate, and is modeled by a thin horizontal crystalline layer submitted to a transverse laser beam. The film is assumed to have a thickness h , and its dimensions in the x and y directions are assumed to be much larger than h . The geometry of the corresponding model is represented in Fig. 1.

Due to thermal heating induced by laser irradiation, an increased vacancy density is created in the subsurface layer. The corresponding transverse vacancy density profile results in a force on the film that may induce bending deformation. Even under uniform irradiation, this system may become unstable versus nonuniform deformations or vacancy density variations. Physically, a local increase in the vacancy density generates a lattice contraction in the film. This contraction has two effects: it locally reduces the defect formation energy, and, furthermore, induces a converging defect flux. As a result, both film contraction and local defect density will

increase. On the other hand, a deformation bump in the film locally decreases the defect density. It furthermore increases the defect formation energy and induces an outgoing defect flux. In this case, a deformation bump will increase while the defect density will decrease. There is thus a feedback loop between local deformation and defect density variations, which provides a destabilizing mechanism for uniform deformations. However, vacancy diffusion tends to wash out non-uniformities in the system and provides a stabilizing mechanism for uniform defect densities. Instability occurs when the feedback loop effects dominate over diffusion, and this instability is of the generation-diffusion-deformation-instability type.⁶

Two nonlinear mechanisms saturate the growth of this instability. The first one comes from finite deformation elasticity, which limits the growth of the deformation. The second one results from vacancy dynamics, where the extra defect flux induced by surface deformation is proportional to the vacancy density. Consequently, defect fluxes from regions of decreasing defect density decrease accordingly in a feedback process, which thus limits defect localization.

Hence, the dynamical model that can describe the evolution of such a system should be based on (i) a nonuniform laser-induced temperature field across the film; (ii) the evolution of vacancy density in strained crystals, including generation and transport; (iii) the deformation of a thin film in the presence of a nonuniform vacancy density. These three aspects are presented next, and are finally assembled in a full dynamical model.

III. LASER-INDUCED HEATING OF THIN FILMS AND TEMPERATURE DISTRIBUTION

Once laser light is absorbed in the thin film, local heating will result in generation and diffusion of lattice defects. We will only consider vacancies as the most likely defects to be generated in metallic films. The concentration of vacancies is heavily dependent on temperature. One thus needs to know how the laser irradiation affects the local temperature of the crystal. We will consider here situations where the laser only heats the material, and that equilibrium between laser radiation and the temperature field is reached on time scales much shorter than the characteristic time scale of vacancy density evolution. Typically, the time scale for equilibration between photon absorption and vacancy generation is on the order of picoseconds, while that for vacancy diffusion is of the order of milliseconds.

The local temperature, $T = T(x, y, z, t) = T(\vec{r}, z, t)$, is determined through the heat conduction equation

$$\frac{\kappa(T)}{D(T)} \partial_t T = \partial_i \kappa(T) \partial_i T + \dot{Q}, \quad (3.1)$$

where $\kappa(T)$ is the thermal conductivity, $D(T)$ is the heat diffusivity ($\kappa = \rho C_p D$ where ρ stands for mass density and C_p for the specific heat at constant pressure), and \dot{Q} is the volumetric laser heating rate. In this case, the source term (\dot{Q}) is calculated assuming that the light energy absorbed by the medium is transformed into heat. In the absence of phase

changes and chemical reactions, and assuming that the laser light propagates in the $-z$ -direction, it may be written as

$$Q(\vec{r}, z, t) = \frac{c}{4\pi} \vec{\nabla} \langle \vec{E} \times \vec{H} \rangle = \vec{k}_l \vec{\nabla} I, \quad (3.2)$$

where I is the time average of the Poynting vector and \vec{k}_l is a unit vector in the direction of the light propagation. If one assumes that the laser beam propagates in the $-z$ direction, the Beer-Lambert law yields

$$\frac{dI(z)}{dz} = \alpha I(z), \quad (3.3)$$

where $\alpha = 4\pi\kappa_a/\lambda$ is the linear absorption coefficient (κ_a is the absorption index and λ the wavelength of the light in vacuum), which defines the absorption length $l_\alpha = \alpha^{-1}$.

The source term may then be written as $Q(\vec{r}, z, t) = I(\vec{r}, t)f(z)$ where I depends on the geometry of the laser beam and $f(z)$ describes the absorption of light along the $-z$ direction. We will consider constant and uniform absorption, and thus $f(z) = \alpha \exp[\alpha(z-h/2)]$.

For the sake of simplicity, we will also consider systems and temperature ranges where κ and D are temperature independent, and, in this case, Eq. (3.1) becomes

$$\partial_t T = D(\Delta + \partial_{zz}^2)T + \frac{\dot{Q}}{\rho C_p} \quad (3.4)$$

(if κ is temperature dependent, this dependence may be eliminated by using the Kirchoff transformation¹⁰)

Of course, this equation has to be supplemented by appropriate boundary conditions. In the following, we will consider two limiting cases. The first case is for systems with no heat losses at the top and bottom boundaries, i.e., where $\eta_{\pm h/2} = 0$ or $\eta h/\kappa \ll 1$, which is a good approximation for typical metallic films in air where $\eta \approx 10^{-4}$ W/cm² K, $\kappa \approx 10^{-1}$ W/cm K. This case corresponds to focused laser irradiation, where heat loss is established on the boundaries of the horizontal x - y plane. The second limiting case is for systems where substrate cooling is strong (e.g., by water or other fluids). This case applies to uniform irradiation, where steady-state temperature profiles can be established by balancing the absorbed laser power with the cooling rate.

A. Focused laser irradiation

Heat dissipation in focused laser heating takes place on the far in-plane zones of the film, with little cooling through the substrate. Under these conditions, we have

$$\partial_z T(\vec{r}, z, t)|_{z=\pm h/2} = 0 \quad (3.5)$$

and the temperature of the film far from the central zone [$T(\infty, 0, t)$] will be taken as the room temperature T_0 . Taking explicitly into account the boundary conditions, the temperature field may be written as

$$T(\vec{r}, z, t) = T_0 + \sum_{n=-\infty}^{+\infty} \int d\vec{q} \frac{1}{2h\pi} \cos \frac{n\pi z}{h} e^{i\vec{q} \cdot \vec{r}} T_{q,n}^-(t) \quad (3.6)$$

and $T_{q,n}^-(t)$ is solution of the equation

$$\partial_t T_{q,n}^-(t) = - \left[q^2 + \left(\frac{n\pi}{h} \right)^2 \right] D T_{q,n}^-(t) + \dot{Q}_{q,n}^-(t), \quad (3.7)$$

where

$$\dot{Q}_{q,n}^-(t) = \int_{-h/2}^{h/2} dz \int d\vec{r} \cos \frac{n\pi z}{h} e^{-i\vec{q} \cdot \vec{r}} \frac{I(\vec{r}, t) f(z)}{\rho C_p} \quad (3.8)$$

and I depends on the type of irradiation (uniform, pulsed, focused, etc.). For $f(z) = \alpha \exp[\alpha(z-h/2)]$, we have

$$\dot{Q}_{q,n}^-(t) = \int d\vec{r} \frac{I(\vec{r}, t)}{\rho C_p} f_n e^{-i\vec{q} \cdot \vec{r}} \quad (3.9)$$

with

$$f_n = \frac{\alpha^2}{\alpha^2 + \left(\frac{n\pi}{h} \right)^2} [1 - (-)^n e^{-\alpha h}]. \quad (3.10)$$

In a few cases of experimental interest, analytical solutions may be obtained for the temperature field. One of these consists in irradiation with a Gaussian CW laser beam of intensity $I(\vec{r}, t) = I_0 \exp[-r^2/r_0^2]$, where I_0 is the maximum beam intensity and r_0 is the beam radius. Performing the integral in Eq. (3.9) and solving Eq. (3.7), we obtain the temperature distribution in Eq. (3.6). In this case, the equilibrium surface temperature distribution becomes, in the high absorption limit ($\alpha h \gg 1$),

$$T_+(\vec{r}) = T(\vec{r}, h/2, \infty) = T_0 + \frac{P(1-R)}{2\sqrt{\pi\kappa r_0}} e^{-(r^2/r_0^2)} I_0 \left(\frac{r^2}{2r_0^2} \right), \quad (3.11)$$

where $I_0(z) = J_0(iz)$ is the zeroth order modified Bessel function. P is the laser power ($P = \pi r_0^2 I_0$) and R is the reflectivity coefficient of the film. This result is in agreement with the Green's-function technique (see Bauerle¹⁰). The temperature increase at the center of the spot is thus¹⁰

$$T_+(\vec{r}) - T_0 = \frac{P(1-R)}{2\sqrt{\pi\kappa r_0}} \quad (3.12)$$

while the transverse temperature profile at the center of the spot is, for $|2z-h| < 2\alpha^{-1}$,

$$T(0, z, \infty) \approx T_0 + \frac{P(1-R)}{2\sqrt{\pi\kappa r_0}} \left[\operatorname{erfc} \left(\frac{2z-h}{2r_0} \right) e^{[(2z-h)/2r_0]^2} - \frac{2}{\alpha r_0^2 \sqrt{\pi}} e^{\alpha[z-(h/2)]} \right] \quad (3.13)$$

and for $|2z-h| > 2\alpha^{-1}$

$$T(0, z, \infty) = T_0 + \frac{P(1-R)}{2\sqrt{\pi\kappa r_0}} \operatorname{erfc} \left(\frac{2z-h}{2r_0} \right) e^{[(2z-h)/2r_0]^2}, \quad (3.14)$$

where erfc is the complementary error function.

B. Uniform laser irradiation

Here, in-plane irradiation is spatially uniform and cooling is provided through the substrate. The in-plane symmetry of uniform irradiation implies that the heat flux vector is only along the z axis, and the problem is simplified as follows. The surface conductance is zero at the upper surface of the film, but is different from zero at the bottom because of substrate cooling. The corresponding boundary conditions are

$$\partial_z T(\vec{r}, z, t)|_{z=+h/2} = 0,$$

$$\partial_z T(\vec{r}, z, t)|_{z=-h/2} = -\frac{\eta}{\kappa} [T(\vec{r}, z, t) - T_0]|_{z=-h/2}. \quad (3.15)$$

With these boundary conditions, the temperature field may be written as

$$T(\vec{r}, z, t) = T(z, t) = T_0 + \sum_{n=-\infty}^{+\infty} \frac{\Lambda_n}{h\Lambda_n + 2\kappa\eta} T_n(t) \cos k_n z, \quad (3.16)$$

where $\Lambda_n = \kappa k_n^2 + \eta^2$ and k_n is defined by the relation $\tan(k_n h) = \eta/\kappa k_n$. $T_n(t)$ is the solution of the equation

$$\partial_t T_n(t) = -k_n^2 D T_n(t) + \dot{Q}_n(t), \quad (3.17)$$

where

$$\dot{Q}_n(t) = \frac{I_a f_n}{\rho C_p} = \frac{I_a}{\rho C_p} \frac{\alpha^2}{\alpha^2 + k_n^2} [1 - \cos(k_n h) e^{-\alpha h}], \quad (3.18)$$

where $I_a = I_0(1-R)$ is the laser-light intensity that is not reflected by the surface. In the high absorption limit, $\alpha h \gg 1$, the temperature profile is then

$$\begin{aligned} T(z, t) &= T_0 + \frac{2I_a}{\kappa} \sum_{n=0}^{+\infty} \frac{\alpha^2}{k_n^2(\alpha^2 + k_n^2)} \frac{\Lambda_n}{h\Lambda_n + 2\kappa\eta} \\ &\quad \times [1 - \exp(-k_n^2 D t)] \cos k_n z \\ &\simeq T_0 + \frac{I_a}{\kappa} \sum_{n=0}^{+\infty} \frac{\alpha^2}{h k_n^2(\alpha^2 + k_n^2)} [1 - \exp(-k_n^2 D t)] \\ &\quad \times \cos k_n z. \end{aligned} \quad (3.19)$$

Since the spectrum of $|k_n|$ has a finite lower bound, which is given by $\tan(k_0 h) = \eta/\kappa k_0$ with $0 < k_0 h < \pi/2$, the temperature profile (3.19) tends to a steady state, given by

$$\begin{aligned} T(z) &= T_0 + \frac{I_a}{\kappa} \left(\frac{h}{2} + z + \frac{e^{-\alpha h}}{\alpha} (1 - e^{\alpha(z+h/2)}) \right. \\ &\quad \left. + \frac{\kappa}{\eta} (1 - e^{-\alpha h}) \right). \end{aligned} \quad (3.20)$$

The top and bottom surface temperatures, T_+ and T_- , are given by

$$T_+ = T_0 + \frac{I_a}{\kappa} \left(h + \frac{e^{-\alpha h}}{\alpha} (1 - e^{\alpha h}) + \frac{\kappa}{\eta} (1 - e^{-\alpha h}) \right),$$

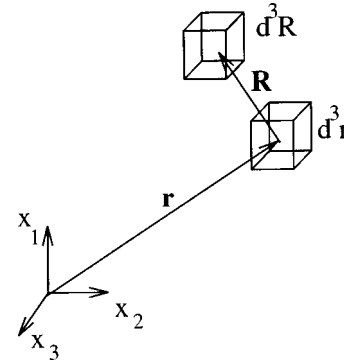


FIG. 2. Definition of the geometrical parameters associated with vacancy transport in strained crystals.

$$T_- = T_0 + \frac{I_a}{\kappa} \left(\frac{1 - e^{-\alpha h}}{\alpha} + \frac{\kappa}{\eta} (1 - e^{-\alpha h}) \right), \quad (3.21)$$

and we may write

$$T(z) = T_+ + (T_+ - T_-) \frac{\alpha \left(z - \frac{h}{2} \right) + 1 - e^{\alpha(z-h/2)}}{\alpha h - 1 + e^{-\alpha h}}. \quad (3.22)$$

For strong surface absorption ($\alpha \gg 1$), the temperature profile is linear and may be written as

$$T(z) = T_+ + \frac{T_+ - T_-}{h} \left(z - \frac{h}{2} \right). \quad (3.23)$$

IV. VACANCY DYNAMICS IN A STRAINED CRYSTAL

Let us analyze first vacancy dynamics in a strained crystal with a nonuniform temperature field. This dynamics is based on vacancy transport, generation, and annihilation.

A. Vacancy transport in a strained crystal

Vacancy transport is evaluated by considering the change in the vacancy concentration $C(\vec{r}, t)$ in a strained crystal with distributed linear absorption sinks (i.e. voids, dislocations, grain boundaries, etc.) In the volume element d^3r , and within the time interval dt , the change in the vacancy population is

$$\Delta C(\vec{r}, t) d^3r. \quad (4.1)$$

We define the following quantities: (1) $\Lambda(\vec{r}|\vec{R})$ is the vacancy jump probability from location \vec{r} to a new location $\vec{R} + \vec{r}$ (cf. Fig. 2) per unit time. (2) $\lambda_v(\vec{r})$ is the probability that a vacancy is absorbed at a homogenized microstructural sink per unit time per sink. (3) $C_s(\vec{r})$ is the concentration of homogenized sinks. (4) $g \exp\{-[E_f(\vec{r})/kT]\}$ is the local rate of vacancy generation in the strained crystal. (5) $E_f(\vec{r})$ is the local vacancy formation energy. (6) g is the entropy of vacancy generation; $g \simeq 1$.

Balancing gains and losses in a volume element d^3r , dividing this relation by $\Delta t d^3r$, and taking the limit for $\Delta t \rightarrow 0$, one has

$$\frac{\partial C}{\partial t} = g \exp\left[-\frac{E_f(\vec{r})}{kT}\right] - \lambda_v(\vec{r}) C_s(\vec{r}) C(\vec{r}) + \frac{1}{V} \int d^3R \times \{C(\vec{r}-\vec{R}, t) \Lambda(\vec{r}-\vec{R}|\vec{R}) - C(\vec{r}, t) \Lambda(\vec{r}|\vec{R})\}, \quad (4.2)$$

where V is the total volume of surrounding neighbors.

Furthermore, we define the local vacancy mean lifetime as

$$\tau(\vec{r}) = 1/\lambda_v(\vec{r}) C_s(\vec{r}). \quad (4.3)$$

If both $C(\vec{r}, t)$ and $\Lambda(\vec{r}|\vec{R})$ change slowly, which is justified away from sharp boundaries, one can expand the product $C(\vec{r}-\vec{R}, t) \cdot \Lambda(\vec{r}-\vec{R}|\vec{R})$ in a Taylor series. At the lowest significant order, one obtains

$$\begin{aligned} \frac{\partial C(\vec{r}, t)}{\partial t} = & g \exp\left[-\frac{E_f(\vec{r})}{kT}\right] - \frac{C(\vec{r}, t)}{\tau(\vec{r})} \\ & - \frac{1}{V} \frac{\partial}{\partial x_i} \left(\int d^3R \Lambda(\vec{r}|\vec{R}) X_i \right) C(\vec{r}, t), \\ & + \frac{1}{V} \frac{\partial^2}{\partial x_i \partial x_j} \left(\int d^3R \Lambda(\vec{r}|\vec{R}) X_i X_j \right) C(\vec{r}, t). \end{aligned} \quad (4.4)$$

Tensor notation and summation over repeated indices are understood throughout the present development.

We further define

$$\vec{F} = \{F_i\} = \frac{1}{V} \int d^3R \Lambda(\vec{r}|\vec{R}) X_i \quad (4.5)$$

and

$$\vec{D} = \{D_{ij}\} = \frac{1}{2V} \int d^3R \Lambda(\vec{r}|\vec{R}) X_i X_j, \quad (4.6)$$

where \vec{F} is the first moment of the jump probability function, or the drift vector for vacancy transport, and D is the second moment of the jump probability function, or the diffusion tensor for vacancy transport.

Substituting Eqs. (4.5) and (4.6) into (4.4), we obtain

$$\begin{aligned} \frac{\partial C(\vec{r}, t)}{\partial t} = & g \exp\left[-\frac{E_f(\vec{r})}{kT}\right] - \frac{C(\vec{r}, t)}{\tau(\vec{r})} + \frac{\partial^2}{\partial x_i \partial x_j} D_{ij}(\vec{r}) C(\vec{r}, t) \\ & - \frac{\partial}{\partial x_i} F_i(\vec{r}) C(\vec{r}, t). \end{aligned} \quad (4.7)$$

Equation (4.7) is now the governing equation for vacancy transport in the thin film. The specific forms of $E_f(\vec{r})$, $\vec{D}(\vec{r})$, and $\vec{F}(\vec{r})$ in a strained crystal remain to be determined.

In a crystal, the jump vector \vec{R} takes on discrete values $\vec{l}^{(\alpha)}$, where α is an index for neighboring positions [i.e., in specific (111), (110), etc. directions]. The integrals in $\vec{D}(\vec{r})$ and $\vec{F}(\vec{r})$ become sums over neighboring positions, of number N :

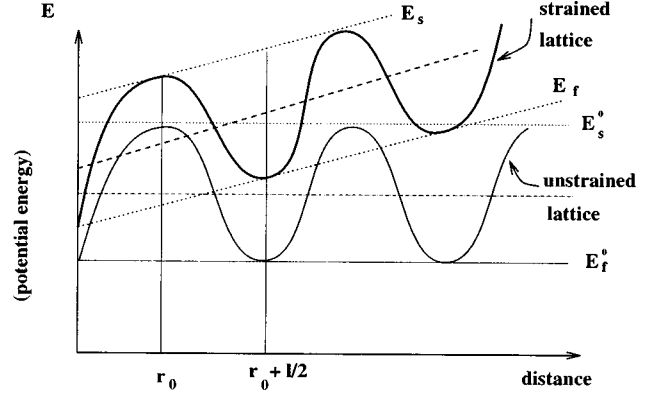


FIG. 3. Schematic spatial variation of the interatomic potential energy of a vacancy in an unstrained and in a strained lattice.

$$F_i = \frac{1}{N} \sum_{\alpha=1}^N \Lambda(\vec{r}|\vec{l}^{(\alpha)}) l_i^{(\alpha)}, \quad (4.8)$$

$$D_{ij} = \frac{1}{2N} \sum_{\alpha=1}^N \Lambda(\vec{r}|\vec{l}^{(\alpha)}) l_i^{(\alpha)} l_j^{(\alpha)}. \quad (4.9)$$

The jump probability will, in a strained lattice (or generally with effects of electric fields or other force fields) depend on the jump direction:

$$\Lambda(\vec{r}|\vec{l}^{(\alpha)}) = \nu_0 \exp\left[-\frac{E_m(\vec{r}, \vec{l}^{(\alpha)})}{kT}\right], \quad (4.10)$$

where $E_m(\vec{r}, \vec{l}^{(\alpha)})$ is the migration energy of the vacancy, which is dependent on the interatomic potential at (\vec{r}) in direction $l^{(\alpha)}$, and ν_0 is the atomic vibrational frequency.

Consider now the variation in the interatomic potential energy of a vacancy in a nonstrained and in a strained lattice, as shown in Fig. 3.

Figure 3 illustrates the variation in vacancy energy in the unstrained (denoted by superscript 0) and the strained crystal. E_f is formation energy, E_s is the saddle-point energy, and E_m is the migration energy, i.e.,

$$E_m(\vec{r}, \vec{l}) = E_s(\vec{r}) - E_f\left(\vec{r} + \frac{\vec{l}}{2}\right). \quad (4.11)$$

Therefore, in a strained lattice, the jump probability takes the form

$$\Lambda(\vec{r}|\vec{l}) = \nu_0 \exp\left[-\frac{E_m(\vec{r}, \vec{l})}{kT}\right], \quad (4.12)$$

$$\Lambda(\vec{r}|\vec{l}) = \nu_0 \exp\left[-\frac{E_s(\vec{r}) - E_f\left(\vec{r} + \frac{\vec{l}}{2}\right)}{kT}\right]. \quad (4.13)$$

We expand the saddle-point energy to first order in \vec{l} , and neglect the difference in the vector length $\vec{l}^{(\alpha)}$ in the deformed and undeformed states.

$$F_i = \nu_0 \exp \left[-\frac{E_m^0(\vec{r})}{kT} \right] \frac{1}{N} \sum_{\alpha=1}^N l_i^{(\alpha)} \left\{ 1 + \frac{1}{2kT} l_j^{(\alpha)} \frac{\partial E_s(\vec{r})}{\partial x_j} \right\} \quad (4.14)$$

and

$$D_{ij}(\vec{r}) = \sum_{\alpha=1}^N \nu_0 \exp \left[-\frac{E_m^0(\vec{r})}{kT} \right] \frac{1}{2N} \times \left\{ 1 - \frac{1}{2kT} l_k^{(\alpha)} \frac{\partial E_s(\vec{r})}{\partial x_k} \right\} l_i^{(\alpha)} l_j^{(\alpha)}, \quad (4.15)$$

where $E_m^0(\vec{r}) = E_s^0(\vec{r}) - E_f^0(\vec{r})$ is the migration energy in an unstrained lattice. Noting that in a FCC crystal $N=12$, $\sum_{\alpha=1}^N l_i^{(\alpha)} l_j^{(\alpha)} = N l^2 \delta_{ij}$, and $\sum_{\alpha=1}^N l_i^{(\alpha)} l_j^{(\alpha)} l_k^{(\alpha)} = 0$, we have

$$F_i = \frac{1}{kT} D_{ij}(\vec{r}) \frac{\partial E_s(\vec{r})}{\partial x_j}, \quad (4.16)$$

where the local diffusion coefficient is defined as

$$D_{ij}(\vec{r}) = \frac{l^2}{6} \nu_0(\vec{r}) \exp \left[-\frac{E_m^0(\vec{r})}{kT} \right] \delta_{ij} = D(\vec{r}) \delta_{ij}. \quad (4.17)$$

Equation (4.7) for vacancy transport finally takes the form

$$\frac{\partial C(\vec{r}, t)}{\partial t} + \vec{\nabla} \cdot \vec{J}(\vec{r}) = g \exp \left[-\frac{E_f(\vec{r})}{kT} \right] - \frac{C(\vec{r}, t)}{\tau(\vec{r})} \quad (4.18)$$

where \vec{J} is the transport flux vector, given by

$$\vec{J}(\vec{r}, t) = - \left[\vec{\nabla} D(\vec{r}) C(\vec{r}, t) - \frac{1}{kT} D(\vec{r}) C(\vec{r}, t) \vec{\nabla} E_s(\vec{r}) \right]. \quad (4.19)$$

The formation and saddle-point energies that appear in these equations depend on the strain, as we will discuss in the next section.

B. Strain field effects on vacancy formation and saddle point energies

For a center of dilatation, the interaction energy in an isotropic elastic medium is given by

$$E_i = -v \sigma_H, \quad (4.20)$$

where v is the relaxation volume of the defect, and σ_H is the hydrostatic component of the stress field.

The relaxation volume of the vacancy is taken as a fraction of the atomic volume, $v = -0.2\Omega$ for a vacancy, Ω being the atomic volume. The interaction energy E_i is the source of the spatial variation in both E_f and E_s , and causes the shift in the interatomic potential. Thus the changes in energy from unstrained to strained crystal are $E^s = E_0^s + E_i$ and $E^f = E_0^f + E_i$. We will also assume that E_0^s and E_0^f are independent of position in the unperturbed crystal.

The hydrostatic stress is given by

$$\sigma_H = \frac{1}{3} \sigma_{ii} = K \epsilon_{ii}, \quad (4.21)$$

where ϵ_{ii} is the first strain invariant, σ_{ii} is the first stress invariant, and K is the bulk modulus. Hence, the interaction energy is $E_i = 0.2\Omega K \epsilon_{ii}$.

Assume that the displacement field is represented by the vector $\vec{U} = (U_1, U_2, U_3)$, then

$$\epsilon_{ii} = \frac{\partial U_1}{\partial x_1} + \frac{\partial U_2}{\partial x_2} + \frac{\partial U_3}{\partial x_3} = \vec{\nabla} \cdot \vec{U}. \quad (4.22)$$

Let $\theta_v = -0.2\Omega K = -0.2b^3 K$ (b is the Burger's vector). Thus,

$$E_i = -\theta_v \vec{\nabla} \cdot \vec{U}. \quad (4.23)$$

Equation (4.23) shows that for a negative volume change (vacancy), the interaction energy is positive. Since $E^s(\vec{r}) = E_0^s - \theta_v \vec{\nabla} \cdot \vec{U}$, its gradient is $\vec{\nabla} E^s(\vec{r}) = -\theta_v \vec{\nabla} (\vec{\nabla} \cdot \vec{U})$. Rearranging Eq. (4.18), we obtain

$$\begin{aligned} \frac{\partial C(\vec{r}, t)}{\partial t} = g \exp \left[-\frac{E_f^0 - \theta_v \vec{\nabla} \cdot \vec{U}}{kT} \right] - \frac{C(\vec{r}, t)}{\tau(\vec{r})} \\ + \nabla_i \nabla_j (D_{ij} C(\vec{r}, t)) + \frac{\theta_v}{kT} \nabla_i (D_{ij} C(\vec{r}, t) \nabla_j (\vec{\nabla} \cdot \vec{U})). \end{aligned} \quad (4.24)$$

Since the change in the formation energy of a vacancy is small compared to the unstrained value, let $C^0(T) = g \exp[-E_f^0/kT]$, and write the generation term as

$$C^0(T) \exp[\theta_v \vec{\nabla} \cdot \vec{U}/kT] \approx C^0(T) \left(1 + \frac{\theta_v}{kT} \vec{\nabla} \cdot \vec{U} \right).$$

If one, furthermore, uses the standard notations

$$\frac{\partial}{\partial t} = \partial_t, \quad \frac{\partial^2}{\partial x^2} = \partial_{xx}^2, \quad \vec{\nabla} = \vec{I}_x \partial_x + \vec{I}_y \partial_y,$$

$$\Delta = \partial_{xx}^2 + \partial_{yy}^2 \quad (4.25)$$

and considers a diffusion tensor where $D_{xx} = D_{yy} = D_{\parallel}$ (the in-plane diffusion coefficient), $D_{zz} = D_{\perp}$ (the transverse diffusion coefficient), the other components being zero, one can rewrite Eq. (4.24) in the form

$$\begin{aligned} \partial_t C = C^0 \left(1 + \frac{\theta_v}{kT} \vec{\nabla} \cdot \vec{U} \right) + D_{\perp} \partial_{zz}^2 C + D_{\parallel} \Delta C - \frac{C}{\tau} \\ + \frac{\theta_v D_{\perp}}{kT} \partial_z (C \partial_z (\vec{\nabla} \cdot \vec{U})) + \frac{\theta_v D_{\parallel}}{kT} \vec{\nabla} \cdot (C \vec{\nabla} (\vec{\nabla} \cdot \vec{U})) \end{aligned} \quad (4.26)$$

V. DEFORMATION EQUATIONS FOR THIN FILMS

In this section, we develop the governing equations for the mechanical deformation of thin films in sufficient detail to allow an exposition of the importance of underlying assumptions. The basic theme in this section is to obtain equations for the relative balance of energy exchanges in the film during its dynamical deformation. We therefore start from a brief description of deformation kinematics, followed by de-

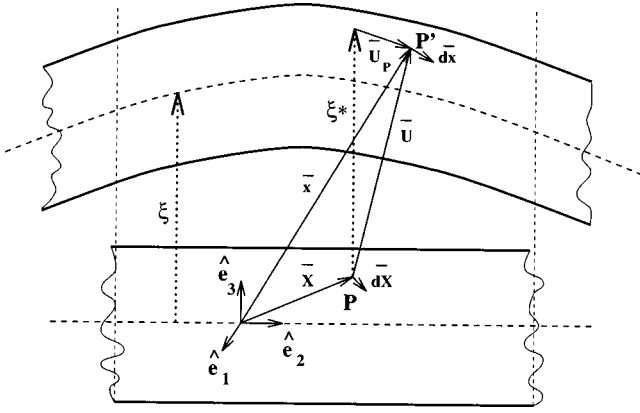


FIG. 4. Definition of geometrical variables in a deformed thin film.

development of equations for the kinetic and strain energy components per unit surface area of the film. We consider three distinct components of the elastic strain energy: the energy stored in bending deformation, the energy stored in stretching deformation, and the energy stored in lattice dilatation (or contraction) as a result of defects.^{11,12}

A. Deformation kinematics

Figure 4 shows the geometry and kinematic variables of a deformed thin film. Here, we use \vec{X} , $d\vec{X}$ as the vector and its increment, which describes a line element at point P in the Lagrangian (material) frame. The element $d\vec{X}$ deforms to $d\vec{x}$ at \vec{x} in the deformed (Eulerian) frame. The transverse translation of P to P' is ξ^* . The displacement vector is \vec{U} . We further decompose \vec{U} into a transverse component ξ^* and an in-plane component \vec{U}_p , i.e.,

$$\vec{U} = \vec{U}_p + \xi^* \vec{e}_3 = \vec{x} - \vec{X}. \quad (5.1)$$

Since the thin film is under simultaneous bending and stretching deformation, we can also write the displacement vector as

$$\vec{U} = \vec{U}_B + \vec{U}_S = \vec{e}_1(U_x + U_\alpha) + \vec{e}_2(U_y + U_\beta) + \vec{e}_3(\xi + d\xi). \quad (5.2)$$

Hence, the transverse displacement is $\xi^* = \xi + d\xi$, where ξ is the transverse displacement of a corresponding point on the midplane. We take $\xi^* \simeq \xi$.

U_x and U_y are the displacement vector components as a result of pure bending, while U_α and U_β are those associated with in-plane stretching by in-plane forces (or stresses $\sigma_{\alpha\beta}$). Before we proceed to evaluate the strain components which follow from the way we prescribed the displacement vector in Eq. (5.2), we state the following underlying assumptions: (1) Since the reference plane is the mid-plane of an isotropic, linearly elastic film, there will be no coupling between bending and stretching strain energy components. (2) Strain tensor components are all computed in the Lagrangian reference frame. The elastic strain energy is independent of the frame, but the in-plane stress tensor components ($\bar{\sigma}_{\alpha\beta}$) must also be

evaluated in the Lagrangian frame. Hence ($\bar{\sigma}_{\alpha\beta}$) is the first Piola tensor, which is nonsymmetric, and is related to the Cauchy stress tensor (σ_{ij}) as

$$\bar{\sigma} = F^{-1} \sigma F \quad (5.3)$$

or

$$\bar{\sigma}_{\alpha\beta} = X_{\alpha,i} \sigma_{ij} x_{\beta,j}. \quad (5.4)$$

(3) Under large deformation, the cross section of the film is assumed to remain planar, thus satisfying the Love-Kirchhoff assumption, and shear stresses are therefore disregarded.

For finite elastic deformation, it can be readily shown that the Lagrangian strain tensor components ϵ_{ij} are given by

$$\epsilon_{ij} = \frac{1}{2}(U_{i,j} + U_{j,i} + U_{k,i}U_{k,j}) \quad (5.5)$$

If we now introduce Eq. (5.2) into Eq. (5.5), we note that the three-term product $U_{k,i}U_{k,j}$ is insignificant for strain components associated with the bending displacements U_x and U_y . For the stretching strains, however, the three-term product has only one significant term, $U_{z,\alpha}U_{z,\beta}$, as a result of large transverse displacements.

B. Strain tensor components

First, let us determine the strain components associated with bending (ϵ_{ij}^B). The bending deformation is characterized by the existence of a neutral surface [characterized by the superscript (0)], which in our case is the midplane of the thin film. The displacement vector for midplane points is given by

$$U_x^{(0)} = U_y^{(0)} = 0, \quad U_z^{(0)} = \xi(x, y). \quad (5.6)$$

Since the film is thin, and only small adhesion forces exist on the bottom surface, then all transverse stress tensor components are nearly zero (plane stress conditions). Therefore, it can be shown¹³ that the nonzero components of the strain tensor are

$$\begin{aligned} \epsilon_{xx}^B &= U_{x,x} = -z\xi_{,xx}, & \epsilon_{yy}^B &= U_{y,y} = -z\xi_{,yy}, \\ \epsilon_{xy}^B &= U_{x,y} = -z\xi_{,xy}, & \epsilon_{zz}^B &= \frac{\nu}{1-\nu}z(\xi_{,xx} + \xi_{,yy}). \end{aligned} \quad (5.7)$$

Now we turn our attention to the strain components associated with stretching the film ($\epsilon_{\alpha\beta}^S$). For pure stretching, the strain tensor is given from Eq. (5.5) as

$$\epsilon_{\alpha\beta}^S = \frac{1}{2}(U_{\alpha,\beta} + U_{\beta,\alpha} + \frac{1}{2}\xi_{,\alpha}\xi_{,\beta}), \quad (5.8)$$

where the indices α and β go over x and y , and summation over repeated indices is understood. The in-plane stretching strain tensor expressed by $\epsilon_{\alpha\beta}^S$ will be associated with an out-of-plane Poisson strain.

Therefore, the in-plane Cauchy stress tensor components, which are associated with stretching, are

$$\sigma_{\alpha\alpha} = \frac{E}{1-\nu^2}(\epsilon_{\alpha\alpha} + \nu\epsilon_{\beta\beta}), \quad \sigma_{\beta\beta} = \frac{E}{1-\nu^2}(\epsilon_{\beta\beta} + \nu\epsilon_{\alpha\alpha}),$$

$$\sigma_{\alpha\beta} = \frac{E}{1+\nu} \epsilon_{\alpha\beta}. \quad (5.9)$$

The strain energy stored in stretching the film can be computed from the strain and stress tensor components developed earlier. In principle, the deformation gradient tensor should contain contributions from thermal expansion, lattice dilatation due to vacancies, and coupled bending strains. Under membrane stretching assumptions, however, the film is reduced to a small volume near the midplane, where bending and defect strains are nearly zero. It will also be shown that the contribution of thermal strains is negligible compared to lattice dilatation by defects.

C. Variational principle for the free energy

Considering the total volume of the thin film, we can write the general form of the first law of thermodynamics as

$$\Delta U^t + \Delta E_K + \Delta E_P = Q + W, \quad (5.10)$$

where ΔU^t is the total elastic strain energy and

$$\Delta U^t = F_B^t + F_S^t + F_D^t, \quad (5.11)$$

where F_B^t is the elastic energy stored in film bending; F_S^t is the elastic energy stored in film stretching; F_D^t is the elastic energy stored in elastic dilatation by defects (vacancies); ΔE_K is the kinetic energy change of the film, equal to $\int_V \frac{1}{2} \rho \bar{U}_{,i} \cdot \bar{U}_{,i} dV$; ΔE_P is the potential energy change (equal to 0 for the present case); Q is the heat added to the film (equal to 0 for steady-state temperature profiles); and W is the work done by external forces, equal to $\int dSP(\xi) d\xi$ (where P is the adhesive force per unit surface area of the film and dS is the surface element area).

Because the film will undergo large deformation in the transverse direction, a simple argument shows that the work done by adhesive forces can be neglected compared to the total elastic energy stored in straining the film. The equilibrium equation describing deformation of the thin film is obtained by considering the total variation in the relevant energy terms of the first law. Thus,

$$\delta F_B^t + \delta F_S^t + \delta F_D^t + \delta E_K = 0. \quad (5.12)$$

We will now consider the total variation in each term separately, and then assemble the terms for the equation of transverse equilibrium.

a. Strain energy of bending. The elastic energy per unit volume is given by¹²

$$F_B = \frac{E}{2(1+\nu)} \left(\epsilon_{ik}^2 + \frac{\nu}{1-2\nu} \epsilon_{ii}^2 \right). \quad (5.13)$$

Substituting the six strain components given by the Eqs. (5.7) into Eq. (5.13) above, we get

$$F_B = z^2 \frac{E}{2(1+\nu)} \left(\frac{1}{1-2\nu} (\xi_{,xx} + \xi_{,yy})^2 + (\xi_{,xy}^2 - \xi_{,xx}\xi_{,yy}) \right). \quad (5.14)$$

Denoting $\xi_{,xx} + \xi_{,yy} = \Delta \xi$, and integrating over the volume of the film, we get

$$F_B^t = \frac{Eh^3}{24(1-\nu^2)} \int \int [(\Delta \xi)^2 + 2(1-\nu)(\xi_{,xy}^2 - \xi_{,xx}\xi_{,yy})] dS. \quad (5.15)$$

Consider now the total variation of δF_B^t as composed of two parts. It can be shown that

$$\begin{aligned} \delta \frac{1}{2} \int dS (\Delta \xi)^2 &= \int dS \delta \xi \Delta^2 \xi - \oint_{\Gamma} dl \delta \xi \frac{\partial \Delta \xi}{\partial n} \\ &+ \oint_{\Gamma} dl \Delta \xi \frac{\partial \delta \xi}{\partial n}, \end{aligned} \quad (5.16)$$

where $\partial/\partial n$ denotes differentiation along the outward normal to the contour bounding the thin film, where Γ represents the contour describing the edge of the film.

We will further assume here that clamped conditions exist on the contour Γ , thus

$$\xi = \delta \xi = \frac{\partial \xi}{\partial n} = 0 \quad (5.17)$$

on Γ .

This condition also allows one to write

$$\begin{aligned} \int \int \{(\xi_{,x,y}^2 - \xi_{,xx}\xi_{,yy})\} dS \\ = \int \int [(q_x q_y)^2 - q_x^2 q_y^2] \xi_{\vec{q}} \xi_{-\vec{q}} d\vec{q} = 0, \end{aligned} \quad (5.18)$$

where $\xi_{\vec{q}}$ is the Fourier transform of $\xi(\vec{r})$.

The total variation in bending energy is finally given by

$$\delta F_B^t = \frac{Eh^3}{12(1-\nu^2)} \int \int \Delta^2 \xi d\xi dS. \quad (5.19)$$

b. Strain energy of stretching. The stretching elastic energy per unit volume is

$$F_S = \frac{1}{2} \epsilon_{\alpha\beta}^S \bar{\sigma}_{\alpha\beta}. \quad (5.20)$$

The in-plane strain components $\epsilon_{\alpha\beta}^S$ are assumed to be uniform within the thickness of the film. Thus the total strain energy in stretching the film is

$$F_S^t = \frac{h}{2} \int \int dS \epsilon_{\alpha\beta} \bar{\sigma}_{\alpha\beta} \quad (5.21)$$

and the total variation is given by¹²

$$\delta F_S^t = -h \int \int dS \{ \bar{\sigma}_{\alpha\beta,\beta} \delta U_{\alpha} + (\bar{\sigma}_{\alpha\beta} \xi_{,\alpha}) \delta \xi \}. \quad (5.22)$$

The first term in the integral is identically zero as a result of in-plane equilibrium in the Lagrangian frame, thus

$$\delta F_S^t = -h \int \int dS (\bar{\sigma}_{\alpha\beta} \xi_{,\alpha}) \delta \xi. \quad (5.23)$$

c. Strain energy stored in lattice dilatation. The energy stored in lattice dilatation per unit volume is given by

$$F_D^v = C \cdot (E_D^0 + E_i^B + E_i^S), \quad (5.24)$$

where E_D^0 is the self-energy per defect, and E_i^B and E_i^S are the components of interaction energy due to bending and stretching, respectively. $E_D^0 \approx \theta_v$. For bending only, one assumes that $\partial_z U_z = \partial_z \xi = 0$, and $\vec{\nabla} \cdot \vec{U} = -mz\Delta\xi$, with $m = 1 - 2\nu/1 - \nu$. Ignoring the contribution of the stretching energy in doing work on the strain field of defects, we get, for the total bending energy stored in lattice dilatation in the thin film,

$$F_D^t \approx \theta_v \int \int \int_{-h/2}^{h/2} [1 + mz\Delta\xi] C dz dS \quad (5.25)$$

and, since $\delta C / \delta \xi = \partial C / \partial \xi$, its variation is

$$\begin{aligned} \delta F_D^t &\approx \theta_v \int \int \int_{-h/2}^{h/2} \left[\frac{\partial C}{\partial z} + zm\Delta C z \right] \delta \xi dz dS, \\ &= \theta_v \int \int [C_+ - C_- + m\Delta I(C)] \delta \xi dS, \end{aligned} \quad (5.26)$$

where $C_+ = C(\vec{r}, h/2, t)$, $C_- = C(\vec{r}, -h/2, t)$, and $I(C) = \int_{-h/2}^{h/2} z C(\vec{r}, z, t) dz$, and up to contour integrals which vanish in clamped conditions, as shown earlier.

For an exponential axial distribution of vacancy concentration, we get

$$\begin{aligned} F_D^v &\approx \theta_v \int \int \left\{ (C_+ - C_-) + m\Delta \int_{-h/2}^{h/2} \right. \\ &\quad \left. \times C_{+z} \exp\left[\gamma\left(z - \frac{h}{2}\right)\right] \right\} \delta \xi dS, \\ &= \theta_v \int \int [\phi + m\psi\Delta] C_+ \delta \xi dS, \end{aligned} \quad (5.27)$$

where $\phi = 1 - \exp(-\gamma h)$ and $\psi = (h/2\gamma)[1 + \exp(-\gamma h)] - (1/\gamma^2)[1 - \exp(-\gamma h)]$.

d. Variation in kinetic energy. The change in the kinetic energy per unit volume is given by

$$\Delta E_K^v = \frac{1}{2} \rho \frac{d\vec{U}}{dt} \cdot \frac{d\vec{U}}{dt}. \quad (5.28)$$

Since the major component of the displacement vector \vec{U} is along the z direction, the velocity vector will be approximated by the time rate of change of the transverse displacement ξ . Thus, per unit area of the film, we have

$$\Delta E_K^S \approx \frac{1}{2} \rho h \dot{\xi}^2. \quad (5.29)$$

The total variation of the kinetic energy of the thin film is given by

$$\delta E_K^t = \frac{1}{2} \rho h \int \int \delta \xi^2 dS = \rho h \int \int \frac{d^2 \xi}{dt^2} d\xi dS. \quad (5.30)$$

e. Equation of motion. From Eq. (5.12) above, and Eqs. (5.19), (5.23), (5.27) and (5.30), and since the displacement and surface elements $d\xi$ and dS are independent, we get

$$\begin{aligned} \partial_t^2 \xi + \frac{Eh^2}{12\rho(1-\nu^2)} \Delta^2 \xi - \frac{1}{\rho} (\bar{\sigma}_{\alpha\beta} \xi_{,\alpha})_{,\beta} \\ = -\frac{\theta_v}{\rho h} [C_+ - C_- + m\Delta I(C)]. \end{aligned} \quad (5.31)$$

The velocity of dilatational acoustic waves is given by

$$c = \sqrt{\frac{E}{\rho(1-\nu^2)}}. \quad (5.32)$$

Since the film is thin, the in-plane first Piola stress tensor variation will be ignored. This will allow us to rewrite the third term in Eq. (5.31) as

$$\frac{1}{\rho} (\bar{\sigma}_{\alpha\beta} \xi_{,\alpha})_{,\beta} = \frac{1}{\rho} \bar{\sigma}_{\alpha\beta} \xi_{,\alpha\beta}. \quad (5.33)$$

The in-plane stress tensor $\bar{\sigma}$ is given by

$$\begin{aligned} \bar{\sigma}_{xx} &= \frac{E}{2(1-\nu^2)} [\xi_{,x}^2 + \nu \xi_{,y}^2 + (1+\nu)\alpha\Delta T + zN_{xx}], \\ \bar{\sigma}_{yy} &= \frac{E}{2(1-\nu^2)} [\xi_{,y}^2 + \nu \xi_{,x}^2 + (1+\nu)\alpha\Delta T + zN_{yy}], \\ \bar{\sigma}_{xy} &= \frac{E}{1+\nu} [\xi_{,x}\xi_{,y} + (1+\nu)\alpha\Delta T + zN_{xy}], \end{aligned} \quad (5.34)$$

and

$$N_{\alpha\beta} = (1-\nu)\xi_{,\alpha\beta} + \nu\delta_{\alpha\beta}\xi_{,\alpha\alpha}. \quad (5.35)$$

In these relationships, the stretching, thermal and bending strains are included. The thermal expansion coefficient is α and ΔT is the average (across the thickness) temperature rise in the film.

If we now define a normalized in-plane stress tensor as

$$\sigma_{\alpha\beta}^* = \frac{1-\nu^2}{E} \bar{\sigma}_{\alpha\beta} \quad (5.36)$$

we finally obtain

$$\partial_t^2 \xi + \frac{c^2 h^2}{12} \Delta^2 \xi - \frac{c^2}{2} \sigma_{\alpha\beta}^* \xi_{,\alpha\beta} = -\frac{\theta_v}{\rho h} [C_+ - C_- + m\Delta I(C)] \quad (5.37)$$

VI. LINEAR STABILITY OF UNDEFORMED STATES UNDER UNIFORM IRRADIATION

A. The dynamical model

Combining the results of the preceding sections, the dynamics of the system may thus be supposed to be governed by the coupled evolution of the vacancy density and the film bending. Neglecting the defect-bending interaction energy ($\kappa \ll 1$) and the stress tensor temperature dependence, since αT is of the order of 10^{-3} in usual experimental conditions, one obtains the model introduced by Emel'yanov:⁶

$$\begin{aligned} \partial_t C = & D_{\perp} \partial_{zz}^2 C + D_{\parallel} \Delta C - \frac{C}{\tau} + \vec{\nabla} \frac{\theta_v D_{\parallel} C}{kT} \vec{\nabla} (\vec{\nabla} \cdot \mathbf{U}) \\ & + \nabla_z \frac{\theta_v D_{\perp} C}{kT} \nabla_z (\vec{\nabla} \cdot \mathbf{U}) + g \exp \left[-\frac{E_f}{kT} \right] (1 + \theta_v \vec{\nabla} \cdot \mathbf{U}) \end{aligned} \quad (6.1)$$

(in usual experimental conditions, $D_{\parallel} \tau \approx 10^{-5}$ cm² and $|\theta_v| \approx 10^{-10}$ erg).

$$\vec{\nabla} \cdot \mathbf{U} = -zm \Delta \xi, \quad (6.2)$$

$$\partial_t^2 \xi + \frac{c^2 h^2}{12} \Delta^2 \xi - \frac{c^2}{2} \sigma_{ij} \partial_{ij}^2 \xi + \frac{\theta_v}{\rho h} (C_+ - C_-) = 0, \quad (6.3)$$

where $C_{\pm} = C(\vec{r}, \pm h/2, t)$ and

$$\sigma_{xx} \approx [(\partial_x \xi)^2 + \nu (\partial_y \xi)^2], \quad (6.4)$$

$$\sigma_{yy} \approx [(\partial_y \xi)^2 + \nu (\partial_x \xi)^2] \quad (6.5)$$

$$\sigma_{xy} \approx -2(1 - \nu) (\partial_x \xi) (\partial_y \xi). \quad (6.6)$$

B. Instability of undeformed states

In this paper, we will analyze the problem of thin films irradiated over large area by cw or pulsed lasers, while focused laser beam irradiation is discussed elsewhere.¹³ Let us then consider the ideal situation of horizontally uniform irradiation of the film surface. We will, furthermore, assume that the temperature profile has reached its equilibrium value. Its evolution is sufficiently slow compared to vacancy generation, and can be considered as quasistationary. In the absence of deformation, the equilibrium vacancy density profile $C^0(z)$ is then the solution of the steady or quasisteady state equation

$$\partial_t C^0 = D_{\perp} \partial_z^2 C^0 - \frac{1}{\tau} C^0 + g \exp \left[-\frac{E_f}{kT(z)} \right], \quad (6.7)$$

with the boundary conditions

$$\partial_z C^0|_{z=h/2} = \partial_z C^0|_{z=-h/2} = 0. \quad (6.8)$$

Hence, the transverse variation of the defect density follows the temperature variation across the film. As discussed in Sec. III, this profile is linear in the limit of strong absorbing layers, and we may write [cf. Eq. (3.23)]:

$$T = T_+ + \frac{T_+ - T_-}{h} \left(z - \frac{h}{2} \right). \quad (6.9)$$

T_+ and T_- are the temperatures of the upper and lower surfaces, respectively, and may be calculated with the method described in Sec. III. $C^0(z)$ behaves thus as

$$C^0(z) \approx C_+^0 \exp \gamma \left(z - \frac{h}{2} \right), \quad (6.10)$$

where $C_+^0 = g \tau \exp[-(E_f/kT_+)]$, when $\gamma \sqrt{D_{\perp} \tau} \ll 1$, with $\gamma = E_f \Delta T / k T_+^2 h$. This gives

$$C^0(h/2) = C_+^0, \quad C^0(-h/2) = C_+^0 e^{-\gamma h} = C_-^0. \quad (6.11)$$

The stability of the undeformed reference state versus spatial perturbations in the horizontal plane is now performed, in order to determine the conditions for deformation patterning instability. Such perturbations are defined as $n(\vec{r}, z, t) = C(\vec{r}, z, t) - C^0(z)$, or, in particular, $n_+(\vec{r}, t) = C_+ - C_+^0$ and $n_-(\vec{r}, t) = C_- - C_-^0 \exp -\gamma h$.

The dynamical model may thus be rewritten as

$$\begin{aligned} \partial_t n_+ = & D_{\parallel} \Delta n_+ - \frac{n_+}{\tau} + \frac{hm \theta_v D_{\parallel}}{2kT_+} \vec{\nabla} (C_+^0 + n_+) \vec{\nabla} \Delta \xi \\ & + \frac{C_+^0}{\tau} \left(1 + \frac{hm \theta_v}{2kT_+} \Delta \xi \right), \end{aligned} \quad (6.12)$$

$$\begin{aligned} \partial_t n_- = & D_{\parallel} \Delta n_- - \frac{n_-}{\tau} - \frac{hm \theta_v D_{\parallel}}{2kT_-} \vec{\nabla} (C_-^0 + n_-) \vec{\nabla} \Delta \xi \\ & + \frac{C_-^0}{\tau} \left(1 - \frac{hm \theta_v}{2kT_-} \Delta \xi \right), \end{aligned} \quad (6.13)$$

$$\begin{aligned} \partial_t^2 \xi = & -\frac{c^2 h^2}{12} \Delta^2 \xi + \frac{c^2}{2} \sigma_{ij} \partial_{ij}^2 \xi - \frac{\theta_v}{\rho h} (n_+ - n_-) \\ & - \frac{\theta_v C_+^0}{\rho h} (1 - e^{-\gamma h}). \end{aligned} \quad (6.14)$$

Note that the transverse variation in the uniform defect density, giving rise to the last term of the right-hand side of Eq. (6.14) is so small that the overall bending it induces is negligible and will not be considered in the following.

On performing the following scalings,

$$\partial_T = \tau \partial_t, \quad \bar{\Delta} = \tau D_{\parallel} \Delta, \quad \mu = \frac{6m \theta_v^2 D_{\parallel} \tau}{\rho c^2 h^2 k},$$

$$\beta = \frac{ch}{\sqrt{12} D_{\parallel}}, \quad \zeta = -\frac{h \theta_v}{2k D_{\parallel} \tau} \xi, \quad N = \mu (n_+ + n_-),$$

$$n = \mu (n_+ - n_-), \quad \epsilon = \mu \left(\frac{C_+}{T_+} + \frac{C_-}{T_-} \right),$$

$$\eta = \mu \left(\frac{C_+}{T_+} - \frac{C_-}{T_-} \right), \quad (6.15)$$

the dynamical model becomes

$$\partial_T N = \Delta N - N - \eta \Delta (\Delta + 1) \zeta - \vec{\nabla} (\chi n + \delta N) \vec{\nabla} \Delta \zeta, \quad (6.16)$$

$$\partial_T n = \Delta n - n - \epsilon \Delta (\Delta + 1) \zeta - \vec{\nabla} (\chi N + \delta n) \vec{\nabla} \Delta \zeta, \quad (6.17)$$

$$\frac{1}{\beta^2} \partial_T^2 \zeta = -\Delta^2 \zeta - n + u \sigma_{ij}(\zeta) \partial_{ij}^2 \zeta, \quad (6.18)$$

where $u = 6(2kTD_{\parallel}\tau/|\theta_v| h^2 \nu)^2$, and where $\chi = T_+ + T_-/2T_+T_-$ and $\delta = T_+ - T_-/2T_+T_-$.

The linear part of this dynamics is thus

$$\partial_T N = \Delta N - N - \delta \Delta (\Delta + 1) \zeta, \quad (6.19)$$

$$\partial_T n = \Delta n - n - \epsilon \Delta (\Delta + 1) \zeta, \quad (6.20)$$

$$\frac{1}{\beta^2} \partial_T^2 \zeta = -\Delta^2 \zeta - n. \quad (6.21)$$

The linear evolution matrix of the coupled deformation-defect system is then, in Fourier transform,

$$\begin{pmatrix} \frac{1}{\beta^2} \omega^2 + \bar{q}^4 & 1 & 0 \\ \epsilon \bar{q}^2 (\bar{q}^2 - 1) & \omega + 1 + \bar{q}^2 & 0 \\ \delta \bar{q}^2 (\bar{q}^2 - 1) & 0 & \omega + 1 + \bar{q}^2 \end{pmatrix}, \quad (6.22)$$

where \bar{q} is the dimensionless wave number, and the corresponding characteristic equation is written

$$(\omega + 1 + \bar{q}^2) \left[\left(\frac{1}{\beta^2} \omega^2 + \bar{q}^4 \right) (\omega + 1 + \bar{q}^2) - \epsilon \bar{q}^2 (\bar{q}^2 - 1) \right] = 0. \quad (6.23)$$

Since, in realistic experimental conditions, $c \approx 10^5$ cm s⁻¹, $h \approx 10^{-2}$ cm, and $D_{\parallel} \approx 10^{-5}$ cm² s⁻¹, one thus has $\beta \gg 1$, and the relevant root for instability is

$$\omega_1 = \epsilon \left(1 - \frac{1}{\bar{q}^2} \right) - (1 + \bar{q}^2). \quad (6.24)$$

Hence, ϵ plays the role of a bifurcation parameter, and, since instability occurs for $\omega_1 \geq 0$, the marginal stability curve is given by

$$\epsilon = \frac{\bar{q}^2 (\bar{q}^2 + 1)}{\bar{q}^2 - 1} \quad (6.25)$$

and the instability threshold is given by

$$\epsilon_c = (1 + \sqrt{2})^2 \approx 5.8, \quad q_c^4 = \epsilon_c, \quad (6.26)$$

where q is the scaled wave number.

Above the instability threshold, there is a band of unstable wave numbers, going from q_m to q_M , where

$$q_{M(m)}^2 = \frac{1}{2} [\epsilon - 1 \pm \sqrt{(B-1)^2 - 4\epsilon}] \quad (6.27)$$

The modes with maximum growth rate correspond to dimensionless wave number $q_0 = \epsilon^{1/4}$, or to unscaled wavelength

$$\lambda_0 = 2\pi \sqrt{\tau D_{\parallel}} \epsilon^{-1/4} = 2\pi l \epsilon^{-1/4} \quad (6.28)$$

Hence, it may be expected that spatial modulations of wave number q equal to or close to q_0 will grow first, leading to the formation of a deformation pattern with a wavelength that is typically of the order of 10 μ m. It is perhaps interesting to recall that, in other pattern-forming systems, the wavelength of the final selected patterns may be different from q_0 , according to nonlinear effects or experimental setups.¹⁵⁻¹⁷ Furthermore, in systems where the band of unstable wave vectors extends to 0 (in infinitely extended systems), such as in spinodal decomposition or in Kuramoto-

Sivashinsky dynamics,¹⁸ patterns are usually transients and develop before the system reaches its final state. In the present case, the film is irradiated by cw lasers or laser pulses. The duration of the pulses limits the evolution of the deformation patterns that should thus result from the growth of the most unstable spatial modes. It is interesting to note that Eq. (6.28) provides a simple physical interpretation of the selected pattern wavelength. The main dependence is on the vacancy mean-free path, with weak contributions from the critical bifurcation parameter. Thus, the wavelength λ_0 is of the order of 10 times the vacancy mean-free path in most systems. In a well-annealed thin film, $\lambda_0 \approx 10$ μ m, with $l \approx 1$ μ m, consistent with experimental observations.^{7,8} However, if other experimental conditions correspond to a thin film that contains a high density of initial defects, the vacancy mean-free path would be short, and the corresponding pattern wavelength small. This finding can be readily tested in appropriate experimental settings.

In isotropic systems, there is an orientational degeneracy in the problem, since the instability threshold and the linear growth rate of the unstable modes only depend on q^2 . Not only all the modes of the unstable band grow, but also unstable modes with any orientation may equally grow. The survivors, and of course the final selected patterns, are determined by their nonlinear interactions. Thus, the nonlinear saturation terms of the dynamics will determine which structure should be selected and what its stability domain should be.

This study evidently requires a nonlinear analysis beyond the instability threshold, which will be presented in subsequent sections. The nonlinear stability we present will be based on the derivation of amplitude equations for patterns close to the instability, and numerical analysis of the model in other regimes.

VII. WEAKLY NONLINEAR ANALYSIS AND PATTERN SELECTION

In the weakly nonlinear regime beyond a pattern forming instability, the dynamics may be reduced to the evolution of an order parameterlike variable that corresponds to the unstable modes.¹⁶ We perform this reduction here, in the framework of the adiabatic elimination of the stable modes.¹⁵ One is the total mean defect density, N , which is the eigenmode corresponding to the eigenvalue $\omega(4) = -(1 + q^2)$ of the linear evolution matrix. The second one is the transverse displacement of the midplane, ζ , that may also be adiabatically eliminated since the characteristic time scale of its evolution, β , is negligibly small. These two variables may thus be expressed, in Fourier transform, as a series expansion in powers of n . This expansion, deduced from the dynamical system (6.16)–(6.18), gives, up to the first relevant contributions,

$$N_{\vec{q}} = \frac{1}{1 + q^2} \left[\eta \left(1 - \frac{1}{q^2} \right) n_{\vec{q}} + \int d\vec{k} \left(\chi + \delta \eta \frac{q^2 - 1}{q^2 (1 + q^2)} \right) \times \frac{\vec{q} \cdot \vec{k}}{k^2} n_{\vec{q} - \vec{k}} n_{\vec{k}} + \dots \right], \quad (7.1)$$

$$\zeta_{\vec{q}} = -\frac{1}{q^4} \left[n_{\vec{q}} - u \int d\vec{k} \int d\vec{k}' \sum_{i,j} E_{ij} n_{\vec{q}-\vec{k}-\vec{k}'} n_{\vec{k}} n_{\vec{k}'} + \dots \right]. \quad (7.2)$$

Using these expressions in the evolution equation for $n_{\vec{q}}$, one finally gets

$$\begin{aligned} \partial_T n_{\vec{q}} = & \omega(q) n_{\vec{q}} + \left(\delta + \eta \chi \frac{q^2 - 1}{q^2(1 + q^2)} \right) \int_c d\vec{k} \frac{\vec{q} \cdot \vec{k}}{k^2} n_{\vec{q}-\vec{k}} n_{\vec{k}} \\ & - \int_c d\vec{k} \int_c d\vec{k}' G(\vec{q}, \vec{k}, \vec{k}') n_{\vec{q}-\vec{k}-\vec{k}'} n_{\vec{k}} n_{\vec{k}'} + \dots, \end{aligned} \quad (7.3)$$

where $\omega(q) = \epsilon(1 - 1/q^2) - (1 + q^2)$, and

$$\begin{aligned} G(\vec{q}, \vec{k}, \vec{k}') = & u \sum_{i,j} E_{ij}(\vec{q}, \vec{k}, \vec{k}') \\ & + \chi \left(\chi + \frac{\delta \eta (q^2 - 1)}{q^2(1 + q^2)} \right) \cdot \frac{(\vec{q} \cdot \vec{k})(\vec{q} - \vec{k}) \cdot \vec{k}'}{k^2 k'^2 (1 + (q - k)^2)}. \end{aligned} \quad (7.4)$$

$E_{ij}(\vec{q}, \vec{k}, \vec{k}')$ are deduced from the nonlinear terms of Eq. (6.18) and write

$$E_{xx}(\vec{q}, \vec{k}, \vec{k}') = \frac{(q - k - k')_x^2 (k_x k'_x + \nu k_y k'_y)}{(q - k - k')^4 k^4 k'^4},$$

$$E_{yy}(\vec{q}, \vec{k}, \vec{k}') = \frac{(q - k - k')_y^2 (k_y k'_y + \nu k_x k'_x)}{(q - k - k')^4 k^4 k'^4}$$

$E_{xy}(\vec{q}, \vec{k}, \vec{k}')$

$$= (1 - \nu) \frac{(q - k - k')_x (q - k - k')_y (k_x k'_y + k_y k'_x)}{(q - k - k')^4 k^4 k'^4}.$$

These integrals are performed on the cylindrical shell of unstable wave vectors.¹⁴ By performing an expansion around the maximum growth rate wave vectors, we finally obtain, up to corrections of the order of $\bar{\epsilon} = (\epsilon - \epsilon_c / \epsilon_c)$ and $(q^2 - q_0^2 / q_0^2)$, which are negligible in the vicinity of the instability,

$$\begin{aligned} \tau_0 \partial_T n_{\vec{q}} = & [\bar{\epsilon} - \Lambda (q^2 - q_c^2)^2] n_{\vec{q}} + \nu \int_c d\vec{k} (\vec{1}_q \cdot \vec{1}_k) n_{\vec{q}-\vec{k}} n_{\vec{k}} \\ & - \int_c d\vec{k} \int_c d\vec{k}' g(\{\vec{1}_q\}) n_{\vec{q}-\vec{k}-\vec{k}'} n_{\vec{k}} n_{\vec{k}'} + \dots, \end{aligned} \quad (7.5)$$

where $\tau_0 = 2 + \sqrt{2}$, $\Lambda = \tau_0 / q_0^2$, $\nu = \tau_0 (\delta + \chi \eta / \epsilon_c)$, and

$$\begin{aligned} g = & \frac{u}{q_0} \sum_{i,j} E_{ij}(\{\vec{1}_q\}) + \tau_0 \chi \left(\chi + \frac{\delta \eta}{\epsilon_c} \right) \cdot (\vec{1}_q \cdot \vec{1}_k) \\ & \times ((\vec{1}_q - \vec{1}_k) \cdot \vec{1}_{k'}) \frac{1}{1 + 2q_0^2 (1 - (\vec{1}_q \cdot \vec{1}_k))} \end{aligned}$$

Hence, $n_{\vec{q}}$ plays the role of an order-parameter-like variable. Since we consider the weakly nonlinear regime in the vicinity of the instability, we may limit the expansion to its cubic term, which is the first relevant contribution for the saturation of the instability. Note that the resulting dynamics present a quadratic contribution, which usually induces sub-critical hexagonal patterns, and cubic contributions which, due to their dependence on the gradients of the order-parameter-like variable, should favor bimodal patterns. We may thus expect that pattern selection and stability will result in a competition between these two types of planforms.¹⁴ In the case of small gradients in temperature and defect density profiles around the midplane of the layer (i.e., $\eta = \delta = 0$) the quadratic term vanishes, and no hexagonal pattern should be expected.

Let us now discuss more precisely pattern selection and stability through analysis of the corresponding amplitude equations, which may be easily obtained from equation (7.5). The simplest pattern one may think of corresponds to stripes, which are defined, in real space, by $n = A e^{iq_0 x} + \bar{A} e^{-iq_0 x}$ (the choice of the wave-vector orientation is arbitrary, as a result of the isotropy of the model, and the following results do not depend on it). The asymptotic evolution of their amplitudes is then given, at the lower order in $\bar{\epsilon}$, by

$$\tau_0 \partial_T A = \bar{\epsilon} A + \zeta_0^2 \partial_x^2 A - g A |A|^2, \quad (7.6)$$

where $\zeta_0^2 = 4q_c^2 \Lambda$, and $g = u \epsilon_c / q_0^8 + (2/1 + 4q_0^2)$.

This equation admits the following family of steady-state solutions:

$$A_0 = \sqrt{\bar{\epsilon} - \zeta_0^2 k^2} e^{i(kx + \Phi)}, \quad (7.7)$$

Φ being an arbitrary phase variable. These solutions are stable versus long-wave-length perturbations in the range, $0 \leq k \leq \sqrt{\bar{\epsilon} / 3 \zeta_0^2}$ (zig-zag and Eckhaus stability limits¹⁶). Furthermore, the stripes with maximum growth rate are the critical ones ($k = 0$).

Due to the structure of the evolution equation (7.5), one has to test the stability of the critical stripe solutions (7.7) versus modulations with wave vectors making an arbitrary angle ϕ with its own wave-vector direction (say, e.g., x), and of amplitude A_ϕ . For $\phi \neq 2\pi/3$, there is no contribution in their dynamics that comes from the quadratic term of Eq. (7.5), and their linear growth rate, in the presence of the stripes (7.7), is then

$$\tau_0 \partial_T A_\phi = \bar{\epsilon} (1 - \gamma(\phi)) A_\phi + \zeta_0^2 (\vec{1}_\phi \cdot \vec{\nabla})^2 A_\phi, \quad (7.8)$$

where

$$\gamma(\phi) = \frac{\frac{4 \cos^2(\phi)}{(1+2q_0^2)^2 - 4q_0^4 \cos^2(\phi)} + \frac{u\epsilon_c}{q_0^8} [2\nu + 2(1-\nu)] \cos^2(\phi)}{\frac{2}{1+4q_0^2} + \frac{u\epsilon_c}{q_0^8}}. \quad (7.9)$$

The first part of this term dominates when the nonlinearities arising from the bending equation are negligible versus the nonlinearities of the defect dynamics (this corresponds to $u \ll 1$ or film thickness $h \geq 5 \mu\text{m}$ in typical experimental conditions), while the second part, which is of the Proctor-Sivashinsky type of coupling,^{17,18} dominates when nonlinearities of defect dynamics become negligible, which is the case for thinner films, such that $u \ll 1$ (or $h \leq 5 \mu\text{m}$ in typical experimental conditions). The maximum growth rate for these modulations corresponds to the minimum of $\gamma(\phi)$, and, for Poisson ratios in the physically acceptable range ($0 \leq \nu \leq 1/2$), $\gamma(\phi)$ is minimum for $\phi = \pi/2$, where it is always less than one. The result of this analysis is that stripes are always unstable, in isotropic systems, versus rectangular bimodal patterns.

The amplitude equations of such patterns, defined as $n = A \exp i q_0 x + B \exp i q_0 y + \text{c.c.}$ are

$$\begin{aligned} \tau_0 \partial_T A &= \bar{\epsilon} A + \zeta_0^2 \partial_x^2 A - g A \left(|A|^2 + \gamma \left(\frac{\pi}{2} \right) |B|^2 \right), \\ \tau_0 \partial_T B &= \bar{\epsilon} B + \zeta_0^2 \partial_x^2 B - g B \left(|B|^2 + \gamma \left(\frac{\pi}{2} \right) |A|^2 \right), \end{aligned} \quad (7.10)$$

and the uniform steady-state solution corresponds to

$$|A|^2 = |B|^2 = \frac{\bar{\epsilon}}{g} \frac{2q_0^8 + \epsilon_c u (1 + 4q_0^2)}{2q_0^8 + \epsilon_c u (1 + 2\nu)(1 + 4q_0^2)}. \quad (7.11)$$

Hence supercritical square structures should be expected in this case, although subcritical hexagonal patterns could, in principle, also develop in the system. Effectively, when $\nu \neq 0$, the structure that is expected to develop subcritically in the dynamics (7.5) corresponds to hexagonal planforms built on modulations with wave vectors making $2\pi/3$ angles between them. In this case the order-parameter-like variable may be written as

$$n = A_1 e^{i\vec{q}_1 \vec{r}} + A_2 e^{i\vec{q}_2 \vec{r}} + A_3 e^{i\vec{q}_3 \vec{r}} + \text{c.c.}$$

with $\vec{q}_1 + \vec{q}_2 + \vec{q}_3 = 0$, $|\vec{q}_i| = q_0$, and the corresponding amplitude equations are¹⁷

$$\begin{aligned} \tau_0 \partial_T A_1 &= \left[\bar{\epsilon} + \frac{\zeta_0^2}{4q_0^2} (\vec{q}_1 \vec{\nabla})^2 \right] A_1 - \frac{\nu}{2} \bar{A}_2 \bar{A}_3 - g A_1 \left(|A_1|^2 \right. \\ &\quad \left. + \gamma \left(\frac{2\pi}{3} \right) (|A_2|^2 + |A_3|^2) \right), \end{aligned}$$

$$\begin{aligned} \tau_0 \partial_T A_2 &= \left[\bar{\epsilon} + \frac{\zeta_0^2}{4q_0^2} (\vec{q}_2 \vec{\nabla})^2 \right] A_2 - \frac{\nu}{2} \bar{A}_1 \bar{A}_3 \\ &\quad - g A_2 \left(|A_2|^2 + \gamma \left(\frac{2\pi}{3} \right) (|A_1|^2 + |A_3|^2) \right), \\ \tau_0 \partial_T A_3 &= \left[\bar{\epsilon} + \frac{\zeta_0^2}{4q_0^2} (\vec{q}_3 \vec{\nabla})^2 \right] A_3 - \frac{\nu}{2} \bar{A}_1 \bar{A}_2 \\ &\quad - g A_3 \left(|A_3|^2 + \gamma \left(\frac{2\pi}{3} \right) (|A_1|^2 + |A_2|^2) \right). \end{aligned} \quad (7.12)$$

Uniform solutions of amplitude

$$\begin{aligned} |A_1| = |A_2| = |A_3| &= \frac{1}{4g \left(1 + 2\gamma \left(\frac{2\pi}{3} \right) \right)} \\ &\times \left[\nu + \sqrt{\nu^2 + 16g \bar{\epsilon} \left(1 + 2\gamma \left(\frac{2\pi}{3} \right) \right)} \right] \end{aligned} \quad (7.13)$$

exist for these equations and are stable for¹⁷

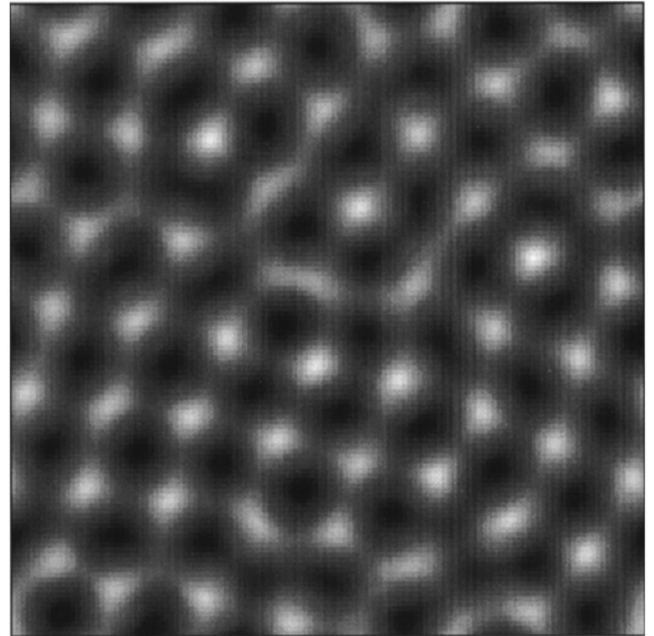


FIG. 5. Squarelike patterns obtained in the numerical analysis of the dynamical model (2.1)–(2.3) for thin-film behavior of the irradiated layer ($u \rightarrow \infty$, $\epsilon = 6.5$, or $\bar{\epsilon} \approx 0.1$).

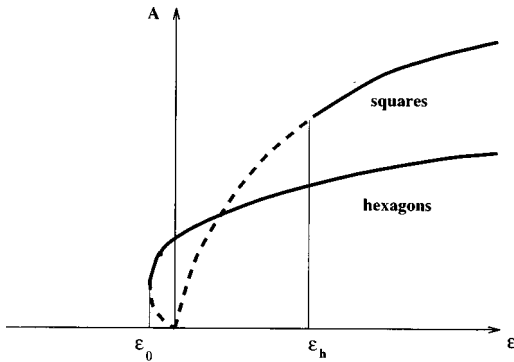


FIG. 6. Bifurcation diagram for uniform solutions of the order-parameter-like dynamics for the “thin film” behavior of the irradiated layer ($u \rightarrow \infty$); plain and dotted lines correspond to stable and unstable states, respectively.

$$-\frac{v^2}{16g \left(1 + 2\gamma \left(\frac{2\pi}{3}\right)\right)} \leq \bar{\epsilon} \leq \frac{3v^2}{16g \left(1 - \gamma \left(\frac{2\pi}{3}\right)\right)^2} \quad (7.14)$$

if $\gamma(2\pi/3) > 1$. If $\gamma(2\pi/3) \leq 1$, they are stable in all the range $-v^2/16g(1 + 2\gamma(2\pi/3)) \leq \bar{\epsilon}$.

Hence, in general, the selected patterns correspond to supercritical squares (see Fig. 5) or subcritical hexagonal planforms. Since usual linear stability analysis shows that squares are unstable versus hexagons for

$$0 \leq \bar{\epsilon} \leq \frac{v^2}{2g \left(\gamma \left(\frac{2\pi}{3}\right) + \gamma \left(\frac{\pi}{6}\right)\right)} = \epsilon_h, \quad (7.15)$$

they may be simultaneously stable for $\bar{\epsilon} > \epsilon_h$ and the corresponding bifurcation diagram is displayed in Fig. 6. Patterns with slightly noncritical wave-vectors may also be stable provided they satisfy phase stability requirements.^{16,19}

When temperature and defect densities are nearly uniform across the film thickness, instability may still occur, but, in this case, there is no quadratic contribution to the nonlinear dynamics of the order-parameter-like variable. Square planforms should thus be observed. However, when the film is thick, $\gamma(\phi) \approx (2 \cos^2 \phi / 1 + a \sin^2 \phi)$, with $a = (4q_0^4 / 1 + 4q_0^2)$ ($a \approx 2.3$ at $\epsilon = \epsilon_c$), according to Eq. (6.26), and square planforms are unstable versus modulations with an angle in the range defined by $\cos^2 \phi = (1 + a) / (2 + a)$. As a result, square planforms are unstable versus modulations with $\phi = \pi/4$, leading to multimodal patterns with wave vectors separated by angles of $\pi/4$, $\pi/2$ and $3\pi/4$. The growth rate of these patterns $[1 - (1/1 + a)]$ is, however, much smaller than the growth rate of hexagonal patterns $[1 - (1/2 + 3a)]$, which are thus expected to be selected in these conditions (see Fig. 7).

For increasing $\bar{\epsilon}$, the range of unstable angles becomes wider, and supercritical hexagonal planforms may in turn become unstable versus patterns built on $n > 3$ pairs of modes, and that are of the quasicrystalline type (see Figs. 8 and 9). Note that these quasiperiodic patterns appear here as a natural consequence of the form of the nonlinear couplings

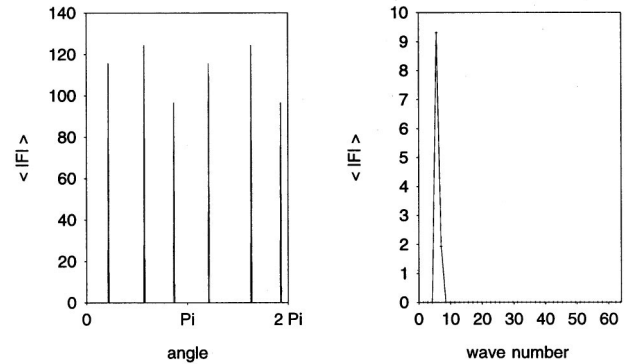
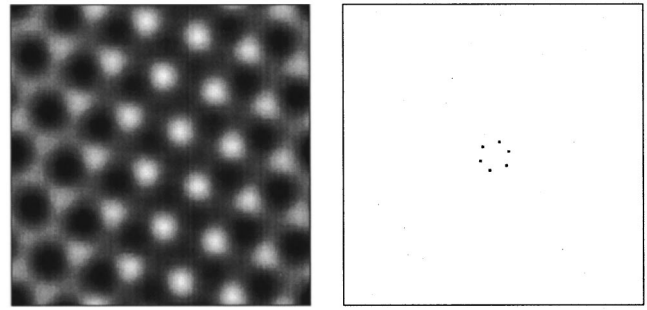


FIG. 7. Supercritical hexagonal patterns obtained in the numerical analysis of the dynamical model (2.1)–(2.3) for plate behavior of the irradiated layer ($u \rightarrow 0$, $\epsilon = 6$, or $\bar{\epsilon} \approx 0.03$).

as suggested in Ref. 21, and do not require particular combinations of external forcings as in other systems.^{22,23}

An important consequence of this analysis is that, in the absence of anisotropy, one-dimensional gratings are always unstable in this dynamics. In systems where the interaction between the laser field and the film surface depends on the crystal symmetries, such gratings could appear, triggered by anisotropic couplings.

It is somewhat surprising to note that instability does not depend on the exact shape of vacancy or temperature profiles across the film. Weakly adherent thin films appear to be unstable for any heating mechanism that generates sufficient concentration of vacancies. Nevertheless, the geometry of the selected patterns depends on such profiles. Furthermore, in transversally uniform systems, nonlinearities are stabilizing while transverse nonuniformities generate destabilizing nonlinearities that accelerate pattern formation, and can overcome even strong substrate adhesion forces.

VIII. NUMERICAL ANALYSIS

The model (6.16, 6.17, 6.18) has been studied numerically for the case when $\eta = \delta = 0$, which rules out subcritical bifurcations, and thus mimics the behavior of uniform systems with negligible transverse temperature gradients. We used an explicit Euler method in Fourier space, with an iterative resolution of the nonlinear deformation equation for the bending coordinate. The system corresponds to 128×128 or 256×256 grids with periodic boundary conditions. The ini-

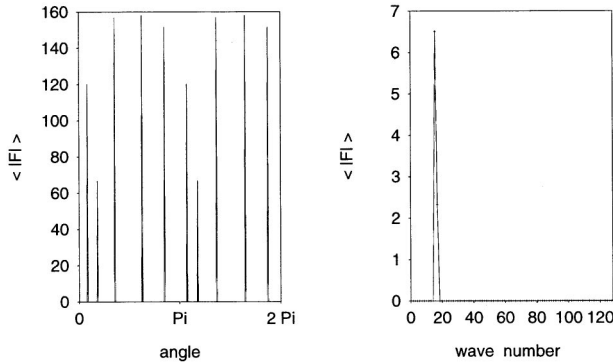
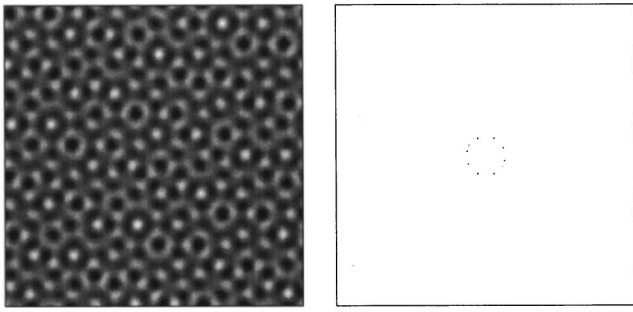


FIG. 8. Patterns with fivefold symmetry obtained in the numerical analysis of the dynamical model for (2.1)–(2.3) for ($u \ll 1$, $\epsilon = 34$, or $\bar{\epsilon} \approx 4.7$).

tial values of the variables were fixed at $N = n = \zeta = 0$ with 1% noise on the n variable. In the thin film regime ($u \gg 1$), square patterns were found, in agreement with analytical results (see Fig. 2). In the “thick” regime ($u \ll 1$), we found the foreseen hexagonal and quasiperiodic patterns. By increasing the bifurcation parameter, we effectively obtained stable patterns with $n = 3, 4, 5, 6$, and 8 pairs of wave vectors. There is thus a basic agreement between the results of the amplitude equation description and the numerical analysis of the complete dynamical system, although quasiperiodic patterns were obtained for relatively high values of the bifurcation parameter. Examples of such patterns are presented in Figs. 7–9. In all these figures, the upper left figure represents the spatial pattern in real space, while the upper right figure corresponds to the same pattern in Fourier space. The lower left and lower right figures, respectively, show the intensity of the Fourier spectrum of the pattern versus wave vector orientation and length. The Fourier spectrum is computed from the numerical solutions of the dynamical model. Besides the good definition of pattern symmetry, one should note the sharp wave-number selection.

IX. DISCUSSION AND CONCLUSIONS

In the first part of this paper, we present a dynamical model for the evolution of perturbations in the vacancy defect density and the associated deformation field in thin films subjected to intense laser irradiation. The present work extends an earlier model by Emel’yanov, and includes a num-

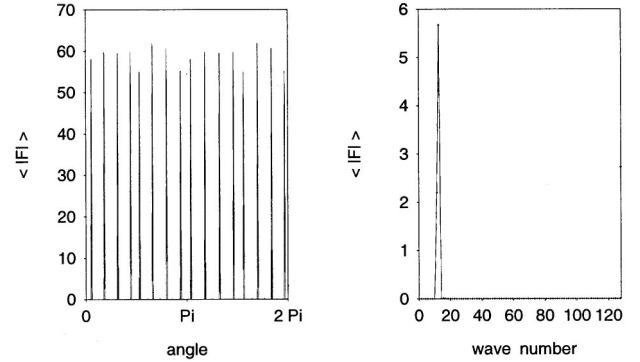
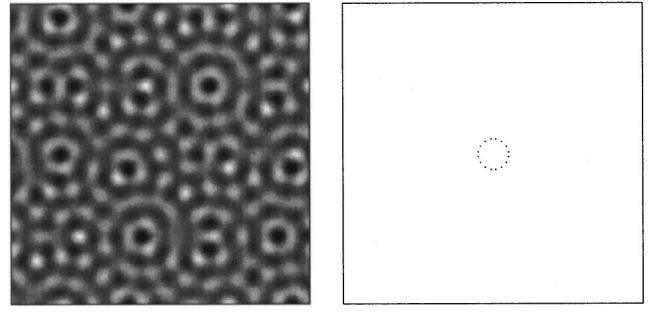


FIG. 9. Patterns with eightfold symmetry obtained in the numerical analysis of the dynamical model (2.1)–(2.3) for ($u \ll 1$, $\epsilon = 38$, or $\bar{\epsilon} \approx 5.4$).

ber of new features, as outlined below.

(1) The field equations for the temperature, defect density and deformation fields are derived in sufficient detail, and in a self-consistent manner. This allows for an examination of the basic assumptions behind the approximations used to develop these governing equations, as well as the range of applicability of the present stability analysis.

(2) The conditions for the necessity of coupling terms between the three components of strain energy (i.e., associated with defects, bending, and stretching) are clarified.

(3) In this new formulation, the dynamical evolution of the transverse displacement of the film’s midplane is explicitly coupled with perturbations in the vacancy concentration at the top and bottom surfaces of the film.

(4) Linear stability analysis of the developed model indicates that the threshold for the mechanical instability of laser irradiated thin films is controlled by the bifurcation parameter ϵ , which can be written as

$$\epsilon = \epsilon_1 \cdot \epsilon_2 \cdot \epsilon_3, \quad (9.1)$$

where

$$\epsilon_1 = \frac{\bar{C} \theta_v}{\rho c^2} \quad (9.2)$$

and \bar{C} is a suitable mean vacancy concentration,

$$\epsilon_2 = \frac{\theta_v}{k\bar{T}}, \quad (9.3)$$

and \bar{T} is a suitable mean temperature,

$$\epsilon_3 = \frac{D_{\parallel}\tau}{h^2} = \left(\frac{l}{h}\right)^2, \quad (9.4)$$

where l is the mean-free path of a vacancy in the thin film.

The physical meaning of the components of the bifurcation parameter are as follows. ϵ_1 is a measure of the ratio of the energy stored in the lattice defects to the kinetic energy associated with sound propagation in the film. The parameter ϵ_2 is a measure of the energy decrease of an atom near a vacancy to its thermal energy, and ϵ_3 is a measure of the ratio of the vacancy mean-free path to the film thickness.

(5) It is now clear that thin film instability is triggered earlier if ϵ_1 , ϵ_2 , or ϵ_3 are increased. This can be achieved experimentally by increasing the laser power (which controls \bar{C} in ϵ_1), or by reducing the concentration of vacancy sinks, thus increasing l in ϵ_3 .

The linear stability analysis derived from the present model is only adequate for studies related to the onset of thin-film instability. However, the nature of selected patterns and their dependence on material and irradiation conditions can only be determined by considering the influence of nonlinear effects in the model, as presented in this paper.

Horizontally uniform vacancy distributions and film deformations are easily shown to become unstable above a threshold value of a bifurcation parameter that combines defect density and temperature, or laser irradiation intensity. The linear analysis determines a preferred wavelength for the deformation patterns that are expected to form beyond the instability.

However, the study of their symmetries, selection, and stability properties require a nonlinear analysis, as performed in Sec. VII, where it appears clearly that pattern selection and stability strongly depend on both linear and nonlinear mechanisms. Special care has thus to be taken on performing nonlinear analysis beyond instability thresholds, especially in the presence of finite-size effects.

In order to reach quantitative agreement with experiments, the model studied here needs to be refined by expressing properly the anisotropies of the system, either in its elas-

tic part and in the diffusion field of vacancies, or by taking into account the possibility of temperature-induced stresses. In pulsed laser irradiation, pattern formation may also depend on the relative importance of the pulse duration and of the growth rate of the unstable modes. Furthermore, since other types of patterns have been observed under irradiation with focused laser beams,^{6,9} it would also be interesting to follow the transition between small finite-size^{6,9,13} (e.g., starlike or roselike patterns) and extended patterns (bands, squares, hexagons, or quasiperiodic) on either increasing the laser irradiation intensity or on decreasing the film thickness. Of course these results require further verification with experimental observations, and systematically designed experimental programs are desirable to this purpose. The nonlinear analysis initiated here is expected to stimulate further research work leading to a better understanding of the formation of deformation patterns on films and surfaces under laser irradiation.

In closing, we list here a number of significant conclusions from the present work.

(1) The selected wavelength of laser-induced patterns is primarily controlled by the vacancy mean-free path, and is in general agreement with experimental observations.

(2) The wavelength can be decreased by starting with a defected film of smaller thickness.

(3) One-dimensional gratings are unstable in a isotropic system. Consistency with experimental observations require anisotropies in the diffusion and elastic fields.

(4) On increasing the bifurcation parameter, square patterns and hexagonal ones are simultaneously stable.

(5) Quasiperiodic patterns are definitively observed to occur in a regime which corresponds to a "thick" film, with small transverse temperature gradients. Since this has not yet been experimentally observed, it would be extremely interesting to produce such "quasicrystalline" structures by testing this regime.

ACKNOWLEDGMENTS

Financial assistance through research grants to UCLA provided by Hughes Research and Lawrence Livermore Laboratories, and the NATO Grant No. CRG-960490 is gratefully acknowledged. D.W. is supported by the Belgian National Fund for Scientific Research.

¹ *Surface Engineering, Surface Modification of Materials*, edited by R. Kossowsky and S. C. Singhal (Martinus Nijhoff, Dordrecht, 1984).

² *Interfaces under Laser Irradiation*, edited by L. Laude, D. Bauerle, and M. Wautelet (Martinus Nijhoff, Dordrecht, 1987).

³ *Patterns, Defects, and Materials Instabilities*, edited by D. Walgraef and N. M. Ghoniem (Kluwer, Dordrecht, 1990).

⁴ *Science and Technology of Thin Film Superconductors*, edited by R. Mc Connell and R. Noufi (Plenum, New York, 1990).

⁵ J. S. Preston, J. E. Sipe, and H. R. van Driel, in *Interfaces under Laser Irradiation*, edited by L. Laude, D. Bauerle, and M. Wautelet (Martinus Nijhoff, Dordrecht, 1987), pp. 127–136.

⁶ V. I. Emel'yanov, *Laser Phys.* **2**, 389 (1992).

⁷ A. F. Banishev, V. I. Emel'yanov, and M. M. Novikov, *Laser Phys.* **2**, 192 (1992).

⁸ J. F. Young, J. S. Preston, H. van Driel, *Phys. Rev. B* **27**, 1141 (1983); **27**, 1155 (1983).

⁹ P. Mogyorosi, K. Piglmayer, and D. Bauerle, *Surf. Sci.* **208**, 232 (1989).

¹⁰ D. Bauerle, *Laser Processing and Chemistry* (Springer-Verlag, New York, 1996).

¹¹ I. W. Boyd, *Laser Processing of Thin Films and Microstructures* (Springer-Verlag, New York, 1987).

¹² L. D. Landau, *Theory of Elasticity*, 3rd ed. (Pergamon Press, Oxford, 1986).

- ¹³J. Lauzeral, D. Walgraef, and N. M. Ghoniem, *Phys. Rev. Lett.* (to be published).
- ¹⁴D. Walgraef, *Spatio-Temporal Pattern Formation* (Springer-Verlag, New York, 1996).
- ¹⁵M. C. Cross and P. C. Hohenberg, *Rev. Mod. Phys.* **65**, 851 (1993).
- ¹⁶P. Borckmans, G. Dewel, A. De Wit, and D. Walgraef, in *Chemical Waves and Patterns*, edited by R. Kapral and K. Showalter (Kluwer, Dordrecht, 1994), pp. 323–363.
- ¹⁷V. L. Gertsberg and G. I. Sivashinsky, *Prog. Theor. Phys.* **66**, 1219 (1981).
- ¹⁸M. R. E. Proctor, *J. Fluid Mech.* **113**, 469 (1981).
- ¹⁹J. Lauzeral, S. Metens, and D. Walgraef, *Europhys. Lett.* **24**, 707 (1993).
- ²⁰D. Walgraef, P. Borckmans, and G. Dewel, *Nature (London)* **318**, 606 (1985).
- ²¹A. C. Newell and Y. Pomeau, *J. Phys. A* **26**, L-429 (1993).
- ²²W. Edwards and S. Fauve, *Phys. Rev. E* **47**, R788 (1993).